arXiv:1510.05603v1 [cond-mat.quant-gas] 19 Oct 2015

Synthetic gauge fields in synthetic dimensions: Interactions and chiral edge modes

Simone Barbarino[1], Luca Taddia[2,3], Davide Rossini[1], Leonardo Mazza[1], and Rosario Fazio[4,1]

[1]NEST, Scuola Normale Superiore & Istituto Nanoscienze-CNR, I-56126 Pisa, Italy
[2]Scuola Normale Superiore, I-56126 Pisa, Italy
[3]CNR - Istituto Nazionale di Ottica, UOS di Firenze LENS, I-50019 Sesto Fiorentino, Italy
[4]The Abdus Salam International Centre for Theoretical Physics (ICTP), I-34151 Trieste, Italy

Abstract. Synthetic ladders realized with one-dimensional alkaline-earth(-like) fermionic gases and subject to a gauge field represent a promising environment for the investigation of quantum Hall physics with ultracold atoms. Using density-matrix renormalization group calculations, we study how the quantum Hall-like chiral edge currents are affected by repulsive atom-atom interactions. We relate the properties of such currents to the asymmetry of the spin resolved momentum distribution function, a quantity which is easily addressable in state-of-art experiments. We show that repulsive interactions significantly stabilize the quantum Hall-like helical region and enhance the chiral currents. Our numerical simulations are performed for atoms with two and three internal spin states.

1. Introduction

One of the most noticeable hallmarks of topological insulators is the presence of robust *gapless edge modes* [1]. Their first experimental observation goes back to the discovery of the quantum Hall effect [2], where the existence of chiral edge states is responsible for the striking transport properties of the Hall bars. The physics of edge states has recently peeked out also in the arena of ultracold gases [3, 4, 5], triggered by the new exciting developments in the implementation of topological models and synthetic gauge potentials for neutral cold atoms [6, 7, 8, 9, 10].

Synthetic gauge potentials in cold atomic systems have already led to the experimental study of Bose-Einstein condensates coupled to a magnetic field [11] or with an effective spin-orbit coupling [12], and more recently to lattice models with non-zero Chern numbers [13, 14, 15, 16] and frustrated ladders [3]. In a cold-gas experiment, the transverse dimension of a two-dimensional setup does not need to be a *physical* dimension, i.e. a dimension in real space: an extra *synthetic* dimension on a given d-dimensional lattice can be engineered taking advantage of the internal atomic degrees of freedom [17]. The crucial requirement is that each of them has to be coupled to

two other states in a sequential way through, for example, proper Raman transitions induced by two laser beams. In this situation, it is even possible to generate gauge fields in synthetic lattices [18].

In this work we focus on one-dimensional systems with a finite synthetic dimension coupled to a synthetic gauge field, i.e. *frustrated ladders*. The study of such ladders traces back to more than thirty years ago, when frustration and commensurate-incommensurate transitions have been addressed in Josephson networks [19, 20]. Thanks to the experimental advances with optical lattices, these systems are now reviving a boost of activity. Both bosonic (see, e.g., Refs. [21, 22, 23, 24, 25]) and fermionic (see, e.g., Refs. [26, 27, 28, 29, 30, 31, 32, 33]) systems have been considered. The emerging phenomenology is amazingly rich, ranging from new phases with chiral order [21] to vortex phases [24] or fractional Hall-like phases in fermionic systems [28, 30], just to give some examples. Very recently, two experimental groups [4, 5] have observed persistent spin currents in one dimensional gases of ^{173}Yb (fermions) and ^{87}Rb (bosons) determined by the presence of such gauge field. Within the framework of the synthetic dimension, such *helical* spin currents can be regarded as the *chiral* edge states of a two-dimensional system and are reminiscent of the edge modes of the Hall effect.

Up to now, the study of edge currents in optical lattices has mainly focused on aspects related to the single-particle physics and a systematic investigation of the interaction effects is missing. Repulsive interactions considerably affect the properties of the edge modes: this is well known in condensed matter, where the fractional quantum Hall regime [34] can be reached for proper particle fillings and for sufficiently strong Coulomb interactions. In view of the new aforementioned experiments in bosonic [5] and fermionic [4] atomic gases, a deeper understanding of the role of repulsive interactions in these setups is of the uttermost importance.

Here we model the experiment on the frustrated n-leg ladder performed in Ref. [4] and analyze, by means of density-matrix renormalization group (DMRG) simulations, how atom-atom repulsive interactions modify the edge physics of the system (in this article we disregard the effects of an harmonic confinement and of the temperature). We concentrate on the momentum distribution function, which has been used in the experiment to indirectly probe the existence of the edge currents. The purpose of this article is twofold. First, we want to present numerical evidence that helical modes, reminiscent of the chiral currents of the integer quantum Hall effect, can be stabilized by repulsive interactions. Second, we want to discuss the influence of interactions on experimentally measurable quantities that witness the chirality of the modes. In this context the words "chiral" and "helical" can be interchanged, depending whether one considers a truly one-dimensional system with an internal degree of freedom or a synthetic ladder. There is an additional important point to be stressed when dealing with synthetic ladders in the presence of interactions. The many-body physics of alkaline-earth(-like) atoms (like Ytterbium) with nuclear spin I larger than $1/2$ is characterized by a SU$(2I+1)$ symmetry [35, 36]. When they are viewed as $(2I+1)$-leg ladders, the interaction is strongly anisotropic, i.e. it is short-range in the physical dimension and

long-range in the synthetic dimension. This situation is remarkably different from the typical condensed-matter systems and may lead to quantitative differences especially when considering narrow ladders, as in Ref. [4].

The paper is organized as follows. In the next section we introduce the model describing a one-dimensional gas of earth-alkaline(-like) atoms with nuclear spin $I \geq 1/2$. In order to make a clear connection with the experiment of Ref. [4], we briefly explain how this system can be viewed as a $(2I+1)$-leg ladder. Moreover, we present a discussion of the single-particle spectrum to understand the main properties of the edge currents in the non-interacting regime and to identify the regimes where the effects of repulsive interactions are most prominent. Then, in Sec. 3 we introduce two quantities, evaluated by means of the DMRG algorithm, that characterize the edge currents: the (spin-resolved) momentum distribution function and the average current derived from it. In Sec. 4 we present and comment our results; we conclude with a summary in Sec. 5.

2. Synthetic gauge fields in synthetic dimensions

2.1. The model

We consider a one-dimensional gas of fermionic earth-alkaline-(like) neutral atoms characterized by a large and tunable nuclear spin I, see Fig. 1(a). Based on the predictions of Ref. [35], Pagano *et al.* have experimentally showed that, by conveniently choosing the populations of the nuclear-spin states, the number of atomic species can be reduced at will to $2\mathcal{I}+1$, giving rise to an effective atomic spin $\mathcal{I} \leq I$ [37]. We stress that I has to be an half-integer to enforce the fermionic statistics, while $\mathcal{I}$ can also be an integer, see Fig. 1(b). Moreover, as extensively discussed in Refs. [17, 18], the system under consideration can be both viewed as a mere one-dimensional gas with $2\mathcal{I}+1$ spin states or as a $(2\mathcal{I}+1)$-leg ladder, see Fig. 1(c).

When loaded into an optical lattice, the Hamiltonian can be written as [35]:

$$\hat{H}_0 = -t \sum_j \sum_{m=-\mathcal{I}}^{\mathcal{I}} \left(\hat{c}^\dagger_{j,m} \hat{c}_{j+1,m} + \text{H.c.} \right) + U \sum_j \sum_{m<m'} \hat{n}_{j,m} \hat{n}_{j,m'} \,, \tag{1}$$

where $\hat{c}_{j,m}$ ($\hat{c}^\dagger_{j,m}$) annihilates (creates) a spin-m fermion ($m = -\mathcal{I}, \ldots, \mathcal{I}$) at site $j = 1, \ldots, L$ and $\hat{n}_{j,m} = \hat{c}^\dagger_{j,m} \hat{c}_{j,m}$; t is the hopping amplitude, while U is the strength of the SU$(2\mathcal{I}+1)$-invariant interaction; the first sum in the hopping term runs over $j = 1, \ldots, L-1$ if open boundary conditions (OBC) in the real dimension are considered, or over $j = 1, \ldots, L$ if periodic boundaries (PBC) are assumed. Hereafter we set $\hbar = 1$. The Hamiltonian (1), also known as the SU$(2\mathcal{I}+1)$ Hubbard model, has attracted considerable attention in the last few decades, see e.g. Refs. [38, 39, 40, 41].

The presence of two additional laser beams can induce a coupling between spin-states with $\Delta m = \pm 1$ of amplitude Ω_m endowed with a running complex phase factor $e^{i\gamma j}$. For simplicity, in the following we assume that Ω_m does not depend on m and set $\Omega_m = \Omega$. The coupling Ω is related to the amplitude of the laser beams, while the

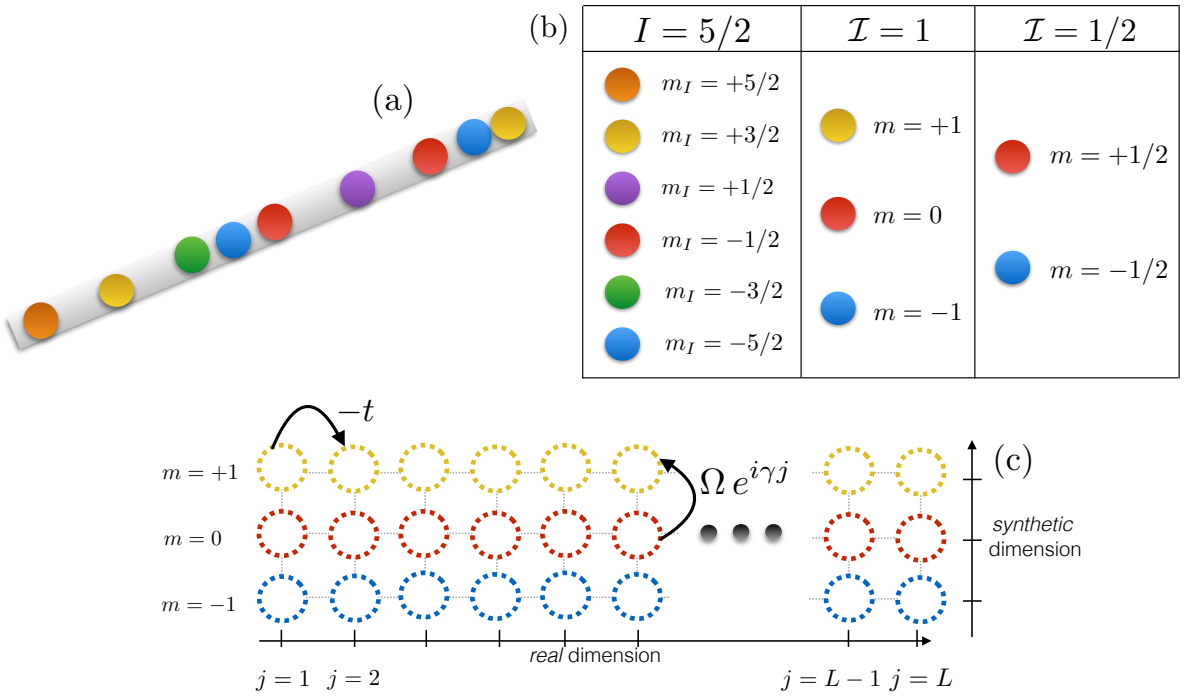

Figure 1. Implementation of $\hat{H} = \hat{H}_0 + \hat{H}_1$ in a cold-atom system. (a) Sketch of a one-dimensional atomic gas with nuclear spin $I = 5/2$, e.g. ^{173}Yb. (b) Definition of the effective spins $\mathcal{I} = 1$ and $\mathcal{I} = 1/2$ as in the experimental implementation with ^{173}Yb of Ref. [4]. (c) Graphical representation of the non-interacting Hamiltonian in the synthetic-dimension picture, for the case $\mathcal{I} = 1$.

phase γ depends on their wavelength and relative propagation angle. Explicitly, the Hamiltonian gets a contribution of the form

$$\hat{H}_1 = \sum_j \sum_{m=-\mathcal{I}}^{\mathcal{I}-1} \Omega_m \left(e^{-i\gamma j} \hat{c}^\dagger_{j,m} \hat{c}_{j,m+1} + \text{H.c.} \right) . \tag{2}$$

As already mentioned, the system characterized by the Hamiltonian $\hat{H} \equiv \hat{H}_0 + \hat{H}_1$ is equivalent to a $(2\mathcal{I}+1)$-leg ladder where the coordinate in the transverse direction is given by the effective-spin index $m = -\mathcal{I}, \ldots, \mathcal{I}$. For all purposes, such direction can be regarded as a synthetic dimension with sharp edges; in this framework, the Hamiltonian $\hat{H}_1$ describes the hopping in the synthetic dimension and introduces a constant magnetic field perpendicular to the ladder with dimensionless magnetic flux $+\gamma$ per plaquette. The peculiarity of our synthetic ladder resides in the interaction term, which is $SU(2\mathcal{I}+1)$ invariant: it therefore describes an on-site interaction in the real dimension and a long-range interaction in the synthetic one.

Since the Hamiltonian $\hat{H}$ is not translationally invariant, for later convenience, we perform the unitary transformation $\hat{d}_{j,m} = \hat{\mathcal{U}} \hat{c}_{j,m} \hat{\mathcal{U}}^\dagger = e^{-im\gamma j} \hat{c}_{j,m}$ such that $\hat{\mathcal{U}}(\hat{H}_0 + \hat{H}_1)\hat{\mathcal{U}}^\dagger = \hat{\mathcal{H}}_0 + \hat{\mathcal{H}}_1 = \hat{\mathcal{H}}$ reads

$$\hat{\mathcal{H}}_0 = -t \sum_j \sum_{m=-\mathcal{I}}^{\mathcal{I}} \left(e^{i\gamma m} \hat{d}^\dagger_{j,m} \hat{d}_{j+1,m} + \text{H.c.} \right) + U \sum_j \sum_{m<m'} \hat{\nu}_{j,m} \hat{\nu}_{j,m'} , \tag{3}$$

$$\hat{\mathcal{H}}_1 = \sum_j \sum_{m=-\mathcal{I}}^{\mathcal{I}-1} \left(\Omega_m \, \hat{d}^\dagger_{j,m} \hat{d}_{j,m+1} + \text{H.c.} \right) , \tag{4}$$

where $\hat{\nu}_{j,m} = \hat{d}^\dagger_{j,m} \hat{d}_{j,m}$. Assuming PBC in the real dimension, the quadratic part of $\hat{\mathcal{H}}$ can be diagonalized in Fourier space, in terms of the operators $\hat{d}_{p,m} = L^{-1/2} \sum_{j=1}^{L} e^{ik_p j} \hat{d}_{j,m}$, with $k_p = 2\pi p/L$ and $p \in \{-L/2, \ldots, L/2 - 1\}$.

2.2. Non-interacting helical liquid

In order to discuss the helical properties of this system, a good starting point is the analysis of the non-interacting physics for the $\mathcal{I} = 1/2$ case. The single-particle spectrum of the Hamiltonian $\hat{\mathcal{H}}$ has two branches with the following dispersion relations:

$$\epsilon_\pm(k_p) = -2t \cos\frac{\gamma}{2} \cos k_p \pm \sqrt{4t^2 \sin^2\frac{\gamma}{2} \sin^2 k_p + \Omega^2} \, . \tag{5}$$

When the condition $\Omega < 2t \sin\frac{\gamma}{2} \tan\frac{\gamma}{2}$ is satisfied, the lower branch displays two minima at $k_p \approx \pm\gamma/2$ and a local maximum at $k_p = 0$, see Fig. 2(a): this case will be referred to as the weak-Raman-coupling (WRC) regime. In the opposite case, dubbed strong-Raman-coupling (SRC) regime, the lower branch has one single minimum at $k_p = 0$ without any special feature at $k_p \neq 0$, see Fig. 2(c).

The study of the spin polarization S^z (related to the operator $\sum_{j,m} m \, \hat{\nu}_{j,m}$) of each eigenmode highlights an important difference between the SRC and the WRC regimes, see Figs. 2(b) and 2(d). In the WRC case, for most of the values of k_p, the eigenstates are prevalently polarized along the z direction, while in the SRC regime this is not true (the dominating polarization is along the x direction, not shown here). Figure 2(a) also shows that in the WRC regime depending on the filling, the low-energy excitation may have very different properties. For low (e.g. the orange line) or high (e.g. the green line) fillings, there are four low-energy excitations. However, when the chemical potential (here we consider zero temperature) lies between $-2t\cos(\gamma/2) - \Omega$ and $-2t\cos(\gamma/2) + \Omega$ (e.g. the violet line), there are two gapless excitations which have definite quasi-momentum and definite spin in the z direction. In the non-interacting case, this is an *helical liquid* which, once interpreted as a ladder, features two chiral edge modes.

Similar considerations about the single-particle spectrum hold for the $\mathcal{I} = 1$ case, even though the analytic form of the eigenenergies is more involved. In Fig. 2(e) we show the single-particle energy spectrum of the eigenstates in the WRC regime. Low, intermediate and high fillings can be identified also in this case, and are indicated by the three different horizontal lines. The intermediate filling (violet line) corresponds to the regime where the helical liquid appears; indeed the spin polarization S^z shown in Fig. 2(f) exhibits almost full polarization of the eigenstates close to the considered Fermi energy. Here, in the synthetic-dimension representation, the three-leg ladder displays chiral modes.

In the interacting case, the spectral properties of the Hamiltonian are not trivially computable. In the following section we define the physical quantities used to properly

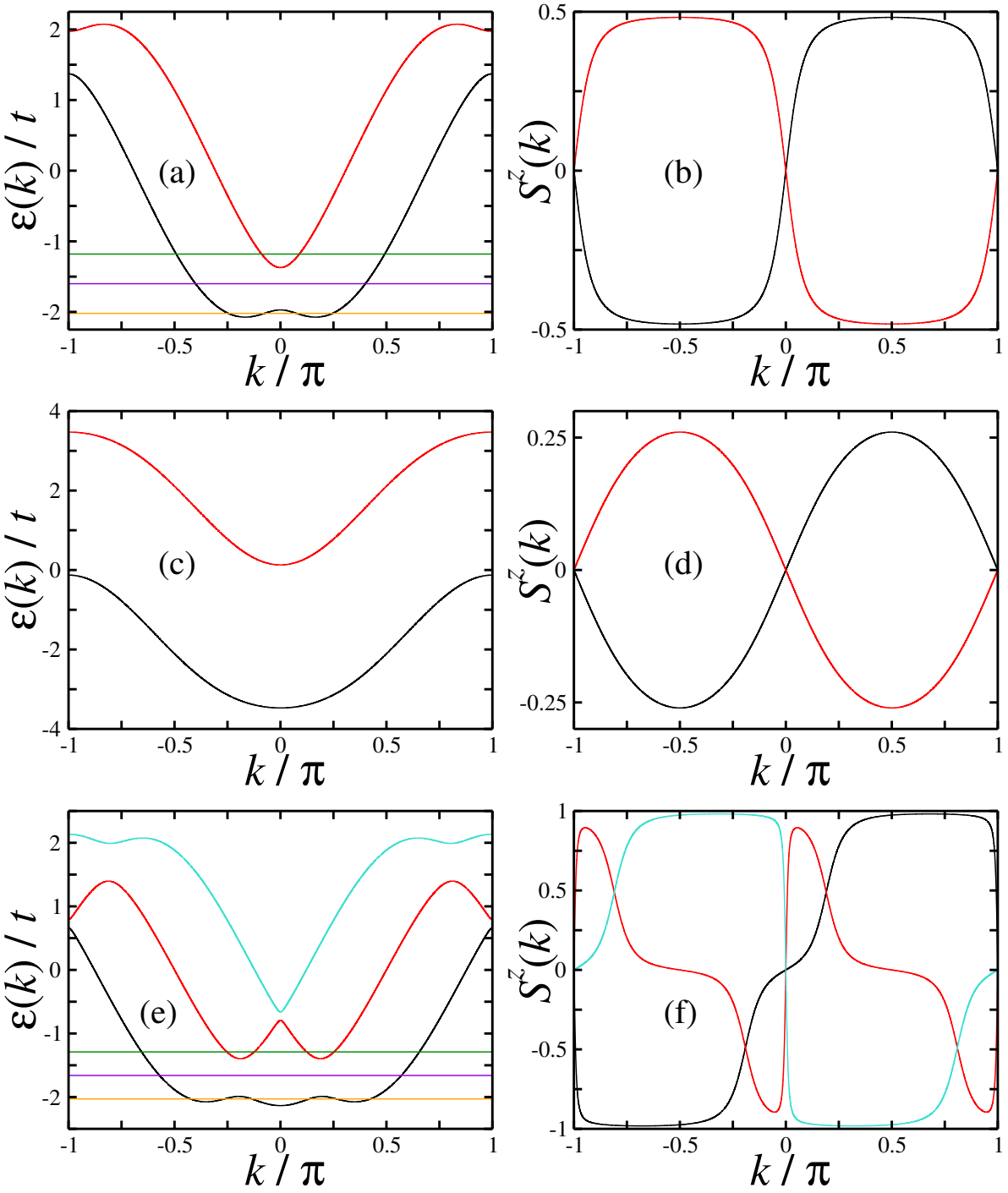

Figure 2. Spectral properties of $\hat{\mathcal{H}}$ in the non-interacting case. Left panels: energy spectra; right panels: spin polarization along the z axis of the quasi-momentum single-particle eigenstates for several cases (lines with the same colors are in correspondence). Panels (a)-(b): $\mathcal{I} = 1/2$ and WRC regime ($\Omega/t = 0.3$). Panels (c)-(d): $\mathcal{I} = 1/2$ and SRC regime ($\Omega/t = 1.8$). Panels (e)-(f): $\mathcal{I} = 1$ and WRC regime ($\Omega/t = 0.1$). In all the situations, we assumed $\gamma = 0.37\pi$, PBC and $L \to \infty$. In panels (a) and (e), the orange, violet and green lines describe, respectively, the low-, intermediate- and high-filling situations considered in the text.

characterize the helical modes, which can be calculated by means of the DMRG algorithm. In the remainder of this paper we carefully analyze such quantities.

3. Observables

The study of the momentum distribution function, both spin-resolved and non-spin-resolved, can provide, as we shall see, information about the helical/chiral nature of the interacting liquid under consideration. The spin-resolved momentum distribution function is defined as

$$n_{p,m} = \langle \hat{c}^\dagger_{p,m} \hat{c}_{p,m} \rangle = \frac{1}{L} \sum_{j,l} e^{-i\frac{2\pi p}{L}(j-l)} \langle \hat{c}^\dagger_{j,m} \hat{c}_{l,m} \rangle \,, \tag{6}$$

where expectation values are taken over the ground state. Since p is not a good quantum number for $\hat{H}$, we will conveniently consider Hamiltonian $\hat{\mathcal{H}}$ and the momentum distribution function $\nu_{p,m} = \langle \hat{d}^\dagger_{p,m} \hat{d}_{p,m} \rangle$, for which it easy to verify that $\nu_{p,m} = n_{p-m\gamma,m}$. Accordingly, the total momentum distribution is given by $n_p = \sum_{m=-\mathcal{I}}^{\mathcal{I}} n_{p,m}$.

Based on these definitions, we introduce two chirality witnesses, i.e. two quantities which diagnose and identify the edge currents determined by the presence of the gauge field $\gamma \neq 0$, even in the presence of repulsive interactions. To this aim, we first solve the continuity equation for the Hamiltonian $\hat{H}$ and define the ground-state average chiral current

$$\mathcal{J}_{j,m} = -i\, t\, \langle \hat{c}^\dagger_{j,m} \hat{c}_{j+1,m} \rangle + \text{H.c.} \,. \tag{7}$$

Assuming PBC in the real dimension and using Eq. (6), its spatial average can be re-expressed as

$$Q_m = \frac{1}{L} \sum_j \mathcal{J}_{j,m} = -\frac{2t}{L} \sum_{p>0} \sin k_p \, (n_{p,m} - n_{-p,m}) \,, \tag{8}$$

with $k_p = 2\pi p/L$. The latter relation allows to indirectly probe the existence of chiral currents using a quantity, namely $n_{p,m}$, which can be experimentally observed in the state-of-art laboratories using a band-mapping technique [42] followed by a Stern-Gerlach time-of-flight imaging [4, 5]. The quantity Q_m is the first chirality witness to be employed in the following.

The second chirality witness is the quantity

$$J_m = -\sum_{p>0} (n_{p,m} - n_{-p,m}) \,, \tag{9}$$

defined in Ref. [4], which is more directly related to the asymmetry of the spin-resolved momentum distribution function. Both J_m and Q_m give information about the circulating currents and, as we shall see below, display the same qualitative behavior (they only differ for a cut-off at low wavelength).

4. Results

Equipped with the definitions given in the previous sections, we now discuss how atom-atom repulsive interactions affect the momentum distribution functions n_p and $n_{p,m}$ and the chirality witnesses Q_m and J_m. The results for the non-interacting cases, here used as a reference, are computed by means of exact diagonalization, while for $U/t \neq 0$ the DMRG algorithm is used [43, 44]. We only address the ground-state properties, i.e. rigorously work at zero temperature. In the finite-size sweeping procedure, up to 250 eigenstates of the reduced density matrix are kept, in order to achieve a truncation error of the order of 10^{-6} (in the worst cases) and a precision, for the computed correlations, at the fourth digit. The resulting inaccuracy is negligible on the scale of all the figures shown hereafter.

Unless differently specified, in the $\mathcal{I} = 1/2$ case we consider $L = 96$ and $\Omega/t = 0.3$, while in the $\mathcal{I} = 1$ case we set $L = 48$ and $\Omega/t = 0.1$ (the ratio Ω/t is chosen in order to be in the WRC regime); $\gamma = 0.37\pi$ coincides with the experimental value of Ref. [4].

As shown in Figs. 2(a) and 2(e), in the non-interacting regime we can outline three inequivalent classes of fillings that we dub low, intermediate and high. In the specific, we consider $N/L = 3/16$, $3/8$ and $7/12$ for $\mathcal{I} = 1/2$, and $N/L = 1/4$, $13/24$ and $5/6$ for $\mathcal{I} = 1$ corresponding to the low-, intermediate-, and high-filling cases respectively. OBC in the real dimension have been adopted.

4.1. Momentum distribution functions

Let us first focus on the $\mathcal{I} = 1/2$ case. In Figs. 3(a-c) we plot the momentum distribution function ν_p for the three fillings listed above. For $U/t = 0$, the behavior of ν_p can be easily predicted by looking at the single-particle spectrum: in the low and high-filling cases peaks arise in correspondence of the partially occupied energy wells, while in the intermediate-filling case a more homogeneous momentum distribution function emerges.

The presence of repulsive atom-atom interactions significantly modifies the momentum distribution functions in the low- and high-filling cases: when U/t is increased, they drive the distribution towards a more homogeneous shape with enhanced tails, a typical effect of interactions [45]. On the contrary, in the intermediate-filling case the homogeneous behavior is unmodified, apart from the mentioned tails. Such a phenomenology is well explained using bosonization and renormalization-group techniques, as discussed in Ref. [46]. Interactions lead to an effective enhancement of the energy of the two gapped modes, whose presence characterizes the helical liquid. Effectively, the interacting system behaves as if Ω/t were renormalized and increased, thus enhancing the filling regimes for which an helical liquid can be expected. Furthermore, this is in agreement with the fact that the non-interacting helical liquid is essentially left unchanged by the interactions. Thus, provided the interaction is sufficiently strong, even low- and high-filling setups can be driven into an helical liquid. This is the first important result of our analysis: repulsive interactions enhance the gap protecting the helical liquid.

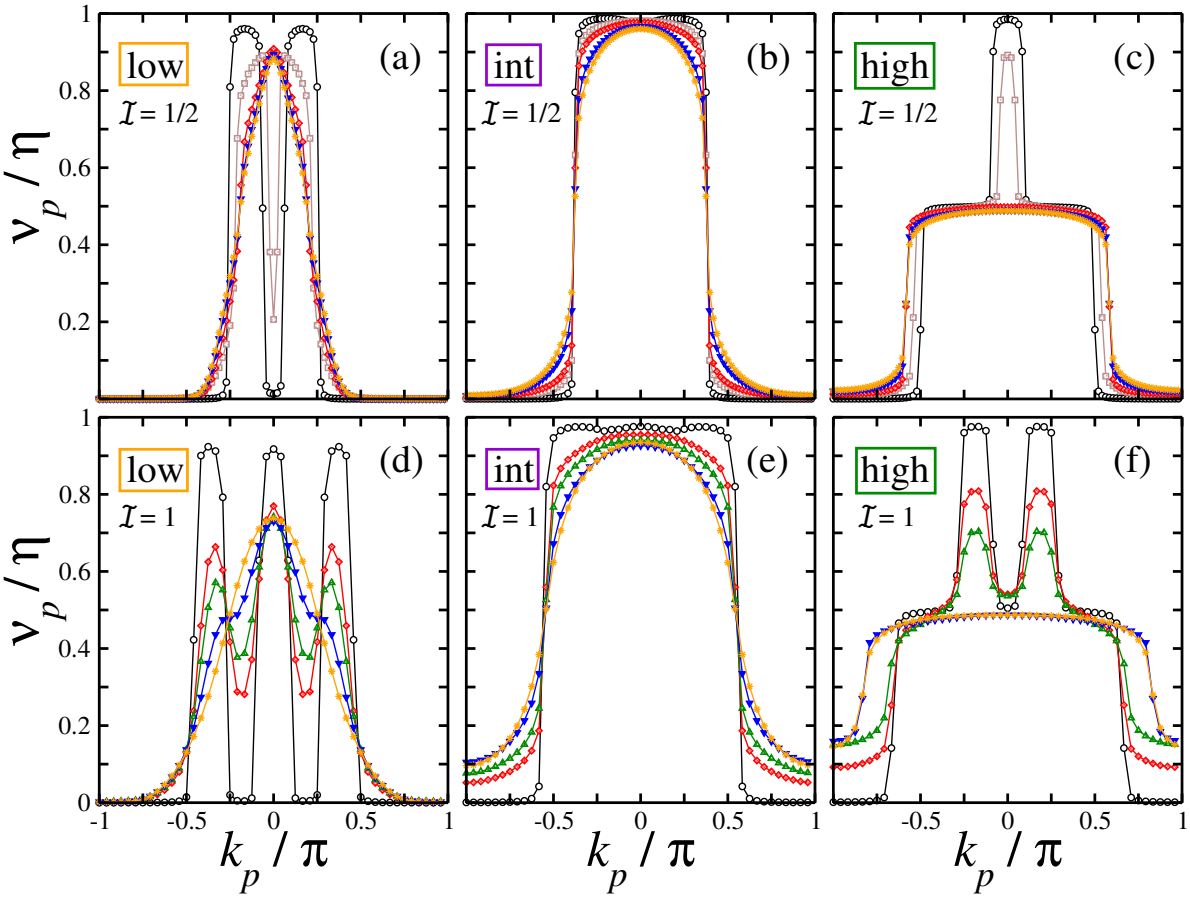

Figure 3. Momentum distribution functions ν_p for different values of the interaction coefficient. First row: $\mathcal{I} = 1/2$; second row: $\mathcal{I} = 1$. First column: low-filling case ($\eta = 1$); second column: intermediate-filling case ($\eta = 1$); last column: high-filling case ($\eta = 2$). The various colors denote different U/t values: 0 (black circles), 3 (brown squares), 5 (red diamonds), 8 (green triangles up), 20 (blue triangles down), $U/t \to \infty$ (orange stars).

The momentum distribution functions for $\mathcal{I} = 1$ at the three cited fillings display the same qualitative behavior, see Figs. 3(d-f). Again, the underlying physics can be explained in terms of an effective enhancement of Ω/t, due to the presence of interactions. Contrary to the previous case, for values of $\mathcal{I}$ larger than $1/2$, no analytical prediction is available, but it seems reasonable to believe that a similar behavior should occur.

It is important to note that in the SRC regime on-site interactions are not expected to significantly modify the momentum distribution function of the non-interacting system. The occupied single-particle states belong only to the lowest band and are almost polarized in the same direction, x: the gas is thus quasi-spinless and an on-site interaction should only weakly alter the ground state because of Pauli exclusion principle. Additional numerical investigations may help in clarifying this issue.

Further information about the system can be revealed by the spin-resolved momentum distribution functions $\nu_{p,m}$. In Figs. 4(a-c) we plot such functions in the WRC regime for the spin species $m = 1/2$ and $\mathcal{I} = 1/2$. Such profiles are clearly

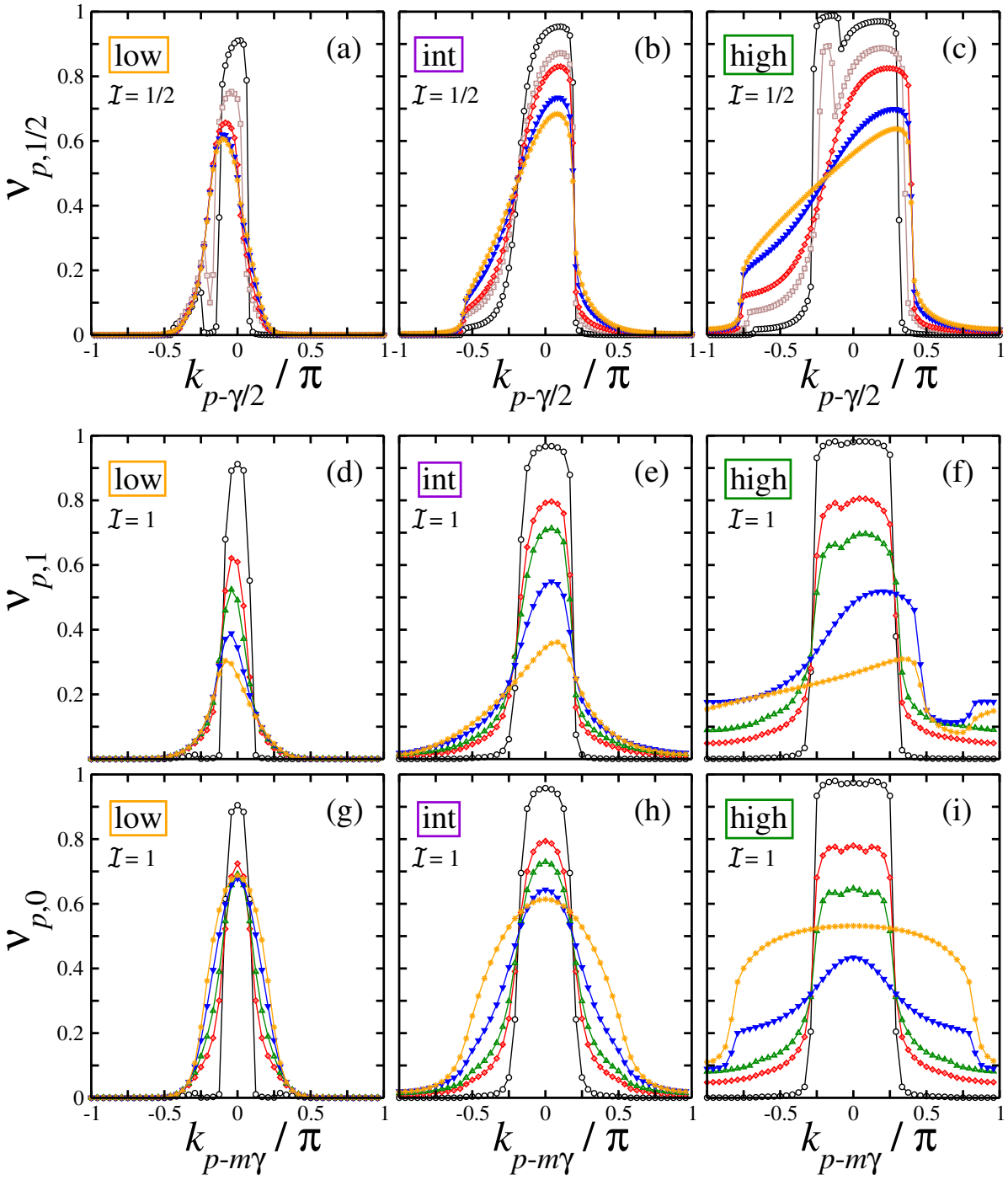

Figure 4. Spin-resolved momentum distribution functions $\nu_{p,m}$ for different values of U/t in the WRC regime. First row: $\mathcal{I} = 1/2$ (note that $\nu_{p,-1/2} = \nu_{-p,1/2}$); second and third row: $\mathcal{I} = 1$ (note that $\nu_{p,-1} = \nu_{-p,1}$). Panels (a), (d) and (g): low-filling case; panels (b), (e) and (h): intermediate-filling case; panels (c), (f) and (i): high-filling case. For the color code, see the caption of Fig. 3.

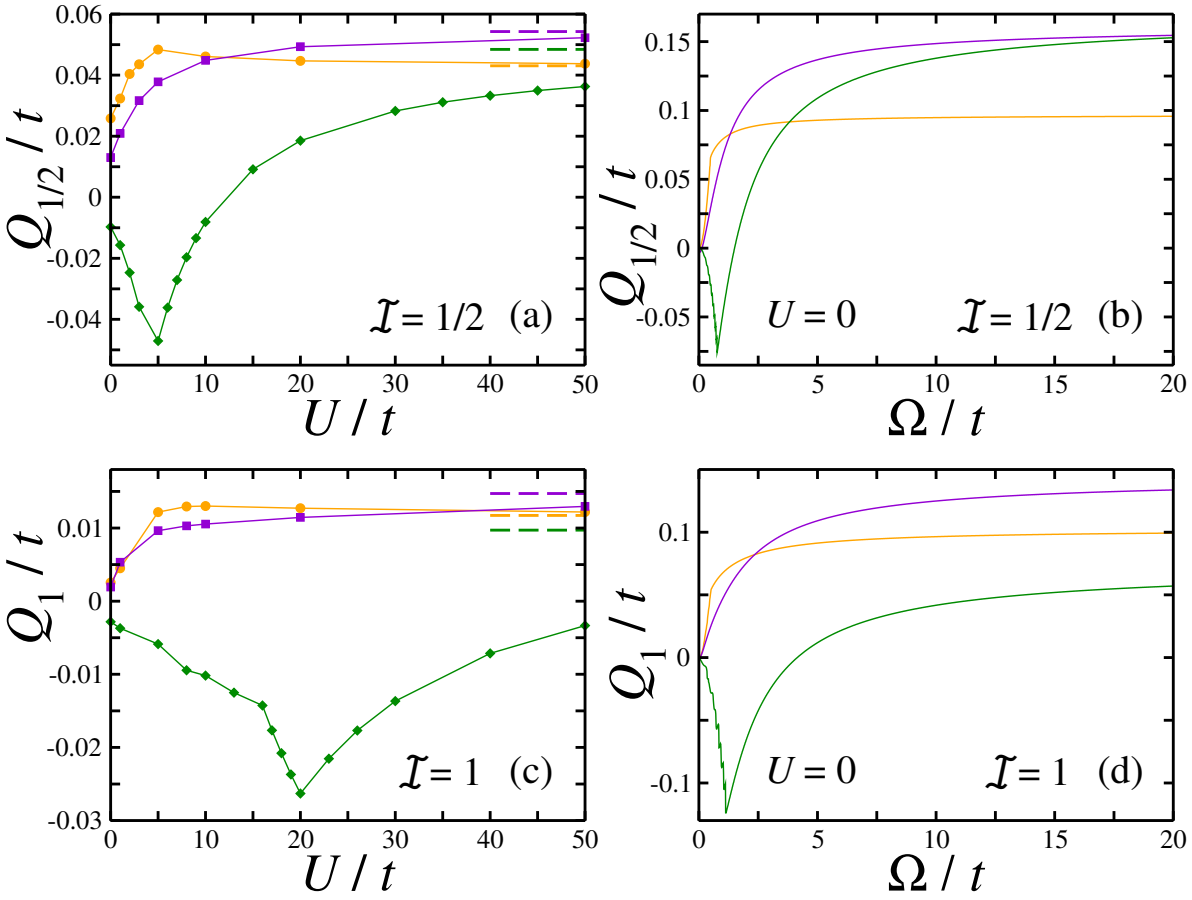

Figure 5. Dependence of $Q_{m=\mathcal{I}}$ on the interaction strength. Panel (a): $Q_{1/2}$ for $\mathcal{I} = 1/2$ as a function of the interaction strength U/t; dashed lines are the values of $Q_{1/2}$ in the limit $U/t \to \infty$. Panel (b): $Q_{1/2}$ for $\mathcal{I} = 1/2$ in the non-interacting case ($U/t = 0$) for different values of Ω/t. Panels (c) and (d): same analysis for $\mathcal{I} = 1$ and $m = 1$. The various curves denote the different regimes of low (orange circles), intermediate (violet squares) and high (green diamonds) filling.

asymmetric with respect to $k_p = 0$, indicating the helical nature of the ground state. Note that the asymmetry is enhanced by the interactions. A similar behavior is observed for $m = \pm 1$ and $\mathcal{I} = 1$, see Figs. 4(d-f). On the other hand, for symmetry reasons, the momentum distribution function $\nu_{p,m=0}$ is symmetric with respect to $k_p = 0$, although it is modified by the interactions, see Figs. 4(g-i).

4.2. Chirality witnesses

In this paragraph we discuss the properties of the chirality witnesses Q_m and J_m for an interacting system. Even though a preliminary analysis of these quantities has been carried out in Ref. [28], a systematic study of the effects of repulsive atom-atom interactions in a relevant experimental setup [4] is still lacking.

In Figs. 5(a) and 5(c) we display the behavior of $Q_{m=\mathcal{I}}$ as a function of U for the cases $\mathcal{I} = 1/2$ and $\mathcal{I} = 1$; we focus again on the three fillings outlined above. In Appendix

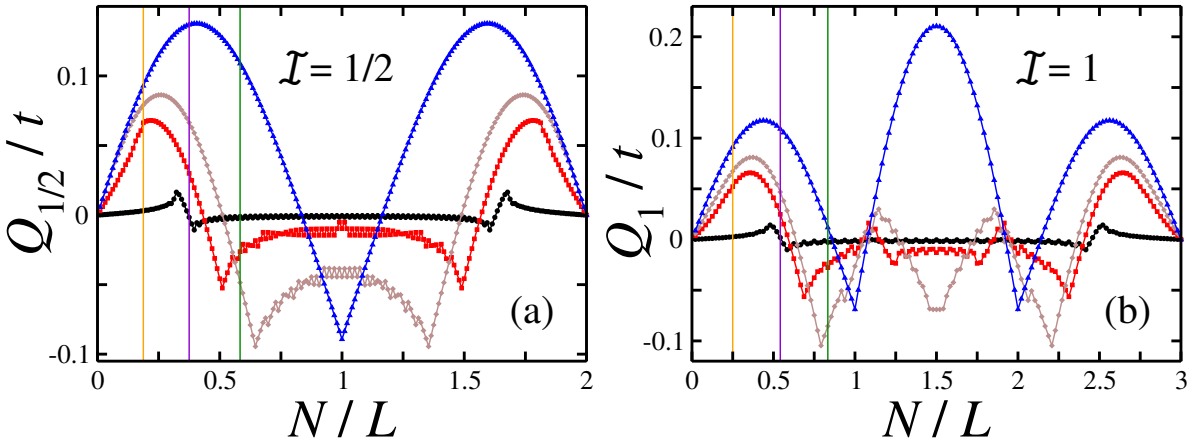

Figure 6. Spatially-averaged currents as a function of the density of atoms. Panel (a): $Q_{1/2}$ for $\mathcal{I} = 1/2$ in the non-interacting case and for different values of Ω (black: $\Omega = 0.1$, red: $\Omega = 0.5$, brown: $\Omega = 1$, blue: $\Omega = 5$); vertical lines mark low, intermediate and high fillings, with the same color code as in Fig. 2(a). Panel (b): same analysis for $\mathcal{I} = 1$ and $m = 1$.

A we show that, although the system has OBC and it is not homogeneous, averaging over many lattice sites yields a value related to the bulk current. A first striking observation is that one can observe different trends, also displaying non-monotonic features. The role of interactions in protecting the helical liquid here encounters a first naive confirmation: in all cases, the value of $|Q_m|$ in the $U/t \to \infty$ limit exceeds that of the non-interacting system.

In order to understand the dependence of Q_m on U/t, we employ an effective model. We have already noticed that the most prominent effect of the interactions on ν_p is that of letting the system behave as if it were non-interacting but with a renormalized value of Ω. Here we test this observation by studying the dependence of Q_m on Ω in the absence of interactions. Results displayed in Figs. 5(b) and 5(d) show that this simple model offers a good qualitative understanding of the interacting system. For example, in both the $\mathcal{I} = 1/2$ and $\mathcal{I} = 1$ cases, $Q_{m=\mathcal{I}}$ displays the same (quasi-)monotonic increasing behavior with U/t and with Ω/t, for the low and intermediate fillings. In the high-filling case, $Q_{m=\mathcal{I}}$ exhibits a strongly non-monotonic behavior as a function of U; in particular the plot points out a change in sign which is *a priori* unexpected because in the classical case the magnetic field determines unambiguously the direction of the circulating currents. To further elucidate this problem, in Fig. 6 we plot the dependence of Q_m on the filling N/L for a fixed value of Ω/t and $U/t = 0$. The plot shows that at low fillings the value of $Q_{m=\mathcal{I}}$ increases gently, but experiences an abrupt decrease once the helical region is entered, marked by the violet line (intermediate fillings). For higher fillings (even outside the helical region) and for small Ω, the value of $Q_{m=\mathcal{I}}$ is negative and thus the current changes sign; however, by increasing Ω, $Q_{m=\mathcal{I}}$ also increases, crossing 0 and becoming positive and finite. It thus follows that in this system the chiral currents are not strictly speaking chiral and states with opposite current flow occur at accessible energies.

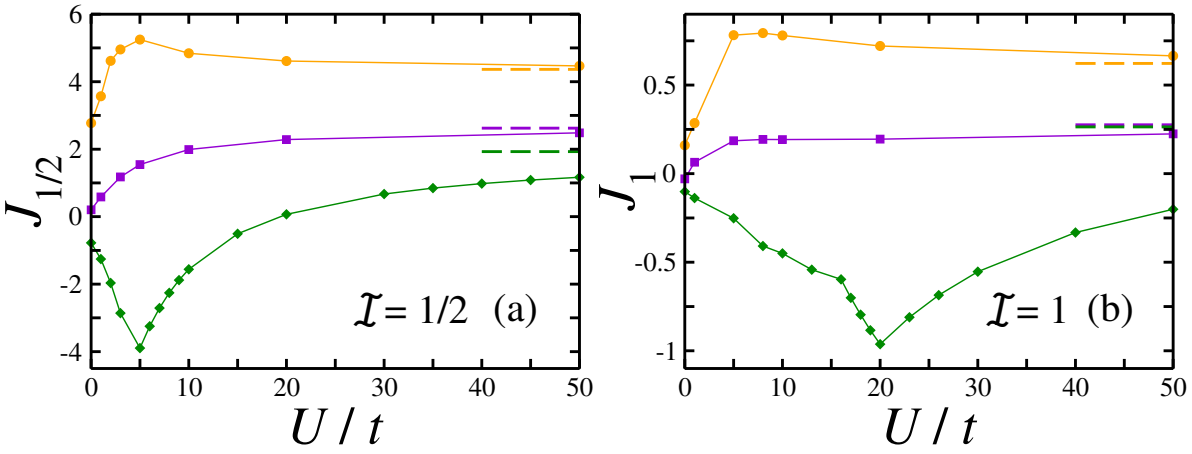

Figure 7. Dependence of $J_{m=\mathcal{I}}$ on the interaction strength. Panel (a): $Q_{1/2}$ for $\mathcal{I} = 1/2$ at low (orange circles), intermediate (violet squares) and high filling (green diamonds) as a function of the interaction strength U/t; dashed lines denote the values of $J_{1/2}$ in the limit $U/t \to \infty$. Panel (b): same analysis for $\mathcal{I} = 1$ and $m = 1$.

The chirality witness $J_{m=\mathcal{I}}$ shares many similarities with $Q_{m=\mathcal{I}}$. In Fig. 7 we plot $J_{m=\mathcal{I}}$ as a function of U, to be compared with Figs. 5(a) and 5(c) for $Q_{m=\mathcal{I}}$. Again, in the low- and intermediate-filling regimes $J_{m=\mathcal{I}}$ is almost monotonous, whereas monotonicity is significantly broken for high fillings. The explanation of this behavior can again be sought in the peculiar dependence of the current carried by the eigenmodes of the system.

5. Conclusions

By means of DMRG simulations, we have studied the impact of atom-atom repulsive interactions on the quantum-Hall-like chiral currents recently detected in Refs. [4, 5]. We have modeled the experimental setup of Ref. [4] and characterized the behavior of the edge currents through the asymmetry of the momentum distribution function.

We have considered different particle fillings and identified the filling range where a chiral/helical liquid appears (in the text dubbed as "intermediate"). When the filling is slightly higher or lower, in the presence of repulsive interactions, the system starts behaving as the non-interacting chiral/helical liquid. This leads to the first conclusion that interactions stabilize such phase. To better assess its nature, we have introduced two chirality witnesses, which are displayed in Figs. 5 and 7, where the chirality of the currents is studied as a function of the interaction strength U/t. As highlighted in the plots, the role of the interaction is non-trivial, and in the strongly-repulsive limit leads to the enhancement of the persistent currents.

In the analysis presented here we have neglected the role of an harmonic trapping confinement as well as finite-temperature effects. Their interplay with interactions and the edge physics highlighted so far is left for a future work.

The edge currents studied here do not have a topological origin. However, these synthetic ladders may support fractional quantum Hall-like states [28, 30], and it would

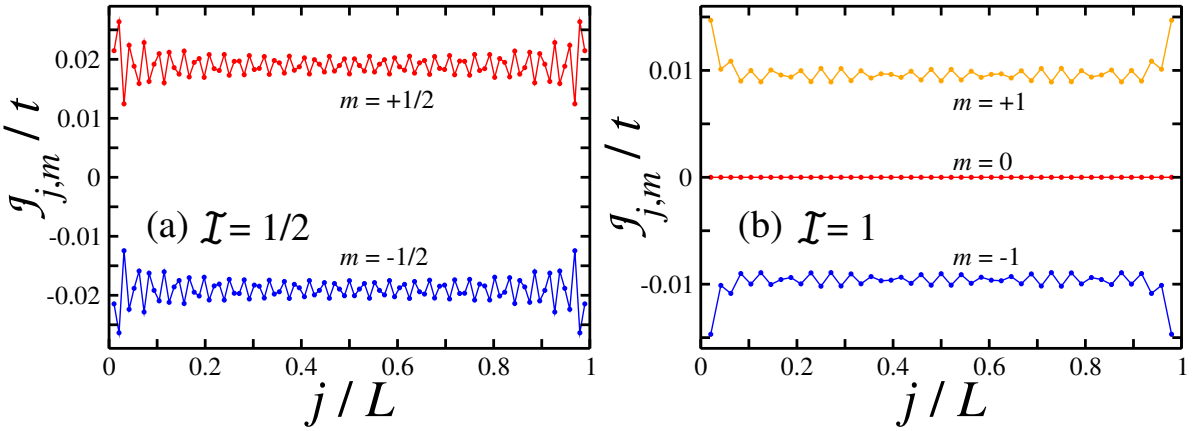

Figure A1. Spatial profile of the spin-resolved currents $\mathcal{J}_{j,m}$. Panel (a): $\mathcal{I} = 1/2$ (blue: $m = -1/2$; red: $m = 1/2$). Panel (b): $\mathcal{I} = 1$ (blue: $m = -1$; red: $m = 0$; orange: $m = 1$). In both cases, intermediate filling and $U/t = 5$ were chosen. The color code refers to Fig. 1. The other parameters of the simulations are set as in Sec. 4.

be very interesting to understand how to explore this regime by means of the quantities discussed in the present paper. In particular it would be important to develop a complete characterization of how fractional quantization may emerge in a cold atomic setup.

Acknowledgements

We thank Leonardo Fallani and Guido Pagano for enlightening discussions, and S. Sinigardi for technical support. We acknowledge INFN-CNAF for providing us computational resources and support, and D. Cesini in particular. We acknowledge financial support from the EU integrated projects SIQS and QUIC, from Italian MIUR via PRIN Project 2010LLKJBX and FIRB project RBFR12NLNA. R.F acknowledges the Oxford Martin School for support and the Clarendon Laboratory for hospitality during the completion of the work.

Appendix A. Currents

The chirality witness Q_m is the space-average value of the expectation value of the current operator over the ground state of the system, $\mathcal{J}_{j,m}$. Whereas in a homogeneous system with PBC this value coincides with the expectation value of the current on every site, the effects of the boundaries in a system with OBC might play an important role.

In Fig. A1 we plot $\mathcal{J}_{j,m}$ both for a system with $\mathcal{I} = 1/2$ [panel (a)] and with $\mathcal{I} = 1$ [panel (b)]. The important information contained in the figure is that even if the system is clearly inhomogeneous, the space pattern of $\mathcal{J}_{j,m}$ is that of a small and fast oscillation over a constant value, so that the space average is an indicative quantity of the underlying physics. For both $\mathcal{I} = 1/2$ and $\mathcal{I} = 1$ the oscillations vanish in the limit $L \to +\infty$, see Ref. [28].

References

[1] Hasan M Z and Kane C L 2010 *Rev. Mod. Phys* **82** 3045; Qi X -L and Zhang S -C 2011 *Rev. Mod. Phys* **83** 1057

[2] Prange R and Girvin S *The Quantum Hall Effect* 1990 Springer New York

[3] Atala M, Aidelsburger M, Lohse M, Barreiro J T, Paredes B and Bloch I 2014 *Nature Phys.* **10** 588

[4] Mancini M, Pagano G, Cappellini G, Livi L, Rider M, Catani J, Sias C, Zoller P, Inguscio M, Dalmonte M and Fallani L 2015 *Science* **349** 1510

[5] Stuhl B K, Lu H -I, Aycock L M, Genkina D and Spielman I B 2015 *Science* **349** 1514

[6] Dalibard J, Gerbier F, Juzeliūnas G and Öhberg P 2011 *Rev. Mod. Phys.* **83**, 1523

[7] Struck J, Ölschläger C, Weinberg M, Hauke P, Simonet J, Eckardt A, Lewenstein M, Sengstock K and Windpassinger P 2012 *Phys. Rev. Lett.* **108** 225304

[8] Hauke P, Tieleman P, Celi A, Ölschläger C, Simonet J, Struck J , Weinberg M, Windpassinger P, Sengstock K, Lewenstein M and Eckardt A 2012 *Phys. Rev. Lett.* **109** 145301

[9] Goldman N, Juzeliunas G, Ohberg P and Spielman I B 2014 *Rep. Prog. Phys.* **77** 126401

[10] Goldman N and Dalibard J 2014 *Phys. Rev. X* **4** 031027

[11] Lin Y -J, Compton R L, Jiménez-García K, Porto J V and Spielman I B 2009 *Nature* **462** 628

[12] Lin Y -J, Jiménez-García K and Spielman I B 2011 *Nature* **471** 83

[13] Aidelsburger M, Atala M, Lohse M, Barreiro J T, Paredes B and Bloch I 2013 *Phys. Rev. Lett.* **111** 185301

[14] Miyake H, Siviloglou G A, Kennedy C J, Burton W C and Ketterle W 2013 *Phys. Rev. Lett.* **111** 185302

[15] Jotzu G, Messer M, Desbuquois R, Lebrat M, Uehlinger T, Greif D and Esslinger T 2014 *Nature* **515** 237

[16] Aidelsburger M, Lohse M, Schweizer C, Atala M, Barreiro J T, Nascimbene S, Cooper N R, Bloch I and Goldman N 2015 *Nature Phys.* **11** 162

[17] Boada A, Celi A, Latorre J I and Lewenstein M 2012 *Phys. Rev. Lett.* **108** 133001

[18] Celi A, Massignan P, Ruseckas J, Goldman N, Spielman I B, Juzeliunas G and Lewenstein M 2014 *Phys. Rev. Lett.* **112** 043001

[19] Kardar M 1984 *Phys. Rev. B* **30** 6368

[20] Kardar M 1986 *Phys. Rev. B* **33** 3125

[21] Dhar A, Maji M, Mishra T, Pai R V, Mukerjee S and Paramekanti A 2012 *Phys. Rev. A* **85** 041602; Dhar A, Maji M, Mishra T, Pai R V, Mukerjee S and Paramekanti A 2013 *Phys. Rev. B* **87** 174501

[22] Petrescu A and Le Hur K 2013 *Phys. Rev. Lett.* **111** 150601

[23] Grusdt F and Höning M 2014 *Phys. Rev. A* **90** 053623

[24] Piraud M, Heidrich-Meisner F, McCulloch I P, Greschner S, Vekua T and Schollwöck U 2015 *Phys. Rev. B* **91** 140406(R)

[25] Tokuno A and Georges A 2014 *New J. Phys.* **16** 073005

[26] Roux G, Orignac E, White S R and Poilblanc D 2007 *Phys. Rev. B* **76** 195105

[27] Sun G, Jaramillo J, Santos L and Vekua T 2013 *Phys. Rev. B* **88** 165101

[28] Barbarino S, Taddia L, Rossini D, Mazza L and Fazio R 2015 *Nature Commun.* **6** 8134

[29] Zeng T -S, Wang C and Zhai H 2015 *Phys. Rev. Lett.* **115** 095302

[30] Cornfeld E and Sela E 2015 *Phys. Rev. B* **92** 115446

[31] Mazza L, Aidelsburger M, Tu H -H, Goldman N and Burrello M 2015 *New J. Phys.* **17** 105001

[32] Budich J C, Laflamme C, Tschirsich F, Montangero M and Zoller P 2015 *arXiv:1505.02800*

[33] Łacki M, Pichler H, Sterdyniak A, Lyras A, Lembessis V E, Al-Dossary O, Budich J C and Zoller P 2015 *arXiv:1507.00030*

[34] Tsui D C, Stormer H L and Gossard A C 1982 *Phys. Rev. Lett.* **48** 1559

[35] Gorshkov A V, Hermele M, Gurarie V, Xu C, Julienne P S, Ye J, Zoller P, Demler E, Lukin M D

and Rey A M 2010 *Nature Phys.* **6** 289
[36] Cazalilla M A and Rey A M 2014 *Rep. Prog. Phys.* **77** 124401
[37] Pagano G, Mancini M, Cappellini G, Lombardi P, Schäfer F, Hu H, Liu X -J, Catani J, Sias C, Inguscio M and Fallani L 2014 *Nature Phys.* **10** 198
[38] Assaraf R, Azaria P, Caffarel M and Lecheminant P 1999 *Phys. Rev. B* **60** 2299
[39] Szirmai E and Sólyom J 2005 *Phys. Rev. B* **71** 205108
[40] Buchta K, Legeza Ö, Szirmai E and Sólyom J 2005 *Phys. Rev. B* **75** 155108
[41] Manmana S R, Hazzard K R A, Chen G, Feiguin A E and Rey A M 2011 *Phys. Rev. A* **84** 043601
[42] Köhl M, Moritz H, Stöferle T, Günter K and Esslinger T 2005 *Phys. Rev. Lett.* **94** 080403
[43] White S R 1992 *Phys. Rev. Lett.* **69** 2863
[44] Schollwöck U 2011 *Ann. Phys.* **96** 326
[45] Giamarchi T *Quantum Physics in One Dimension* 2003 Oxford University Press
[46] Braunecker B, Japaridze G I, Klinovaja J and Loss D 2010 *Phys. Rev. B* **82** 045127